Search for two-neutrino double-β decay of ^{96}Zr to excited states of ^{96}Mo

S. W. Finch and W. Tornow

Phys. Rev. C **92**, 045501 — Published 8 October 2015

DOI: 10.1103/PhysRevC.92.045501

Search for two-neutrino double-β decay of ^{96}Zr to excited states of ^{96}Mo

S.W. Finch* and W. Tornow
Department of Physics, Duke University, Durham, North Carolina 27708, USA
and Triangle Universities Nuclear Laboratory, Durham, North Carolina 27708, USA

Background: Double-β decay is a rare second-order nuclear decay. The importance of this decay steams from the possibility of neutrinoless double-β decay and its applications to neutrino physics.

Purpose: A search was conducted for the $2\nu\beta\beta$ decay of ^{96}Zr to excited final states of the daughter nucleus, ^{96}Mo. Measurements of this decay are important to test nuclear matrix element calculations, which are necessary to extract the neutrino mass from a measurement of the neutrinoless double-β decay half-life.

Method: Two coaxial high-purity germanium detectors were used in coincidence to detect γ rays produced by the daughter nucleus as it de-excited to the ground state. The experiment was carried out at the Kimballton Underground Research Facility and produced 685.7 days of data with a 17.91 g enriched sample.

Results: No counts were seen above background. For the decay to the first excited 0^+ state, a limit of $T_{1/2} > 3.1 \times 10^{20}$ yr was produced. Limits to higher excited states are also reported.

Conclusion: The new limits on double-β decay are an improvement over previous experiments by a factor of 2 to 5 for the various excited states. The nuclear matrix element for the double-β decay to the first excited 0^+ state is found to be < 0.13.

I. INTRODUCTION

Two-neutrino double-β ($2\nu\beta\beta$) decay is a rare standard model decay in which two nuclear neutrons decay into two protons with emission of two electrons and two antineutrinos. There is currently a large interest in double-β decay due to the possibility of detecting the lepton number violating neutrinoless double-β ($0\nu\beta\beta$) decay mode. Observation of this decay would illuminate the Majorana or Dirac nature of the neutrino.

The half-life of $2\nu\beta\beta$ and $0\nu\beta\beta$ decay are described by

$$(T^{2\nu}_{1/2})^{-1} = G_{2\nu}(Q_{\beta\beta}, Z)|M^{2\nu}|^2 \,, \quad (1)$$

$$(T^{0\nu}_{1/2})^{-1} = G_{0\nu}(Q_{\beta\beta}, Z)|M^{0\nu}|^2\langle m_{\beta\beta}\rangle^2 \,, \quad (2)$$

respectively [1]. $G(Q_{\beta\beta}, Z)$ contains the phase-space integrals, $|M|$ is the nuclear matrix element (NME), and $\langle m_{\beta\beta}\rangle$ is the effective Majorana mass of the electron neutrino. Although neutrino oscillation experiments have proven that neutrinos have mass and measured their mass squared differences, only upper limits exists for the absolute neutrino mass. Should a measurement of $0\nu\beta\beta$ be made, it would allow for determination of the effective neutrino mass. This requires precise theoretical calculations of the NME. Experimentally measured $2\nu\beta\beta$ decay half-lives are necessary to tune and verify NME calculations. Measuring the decay mode to excited nuclear states gives additional information on the nuclear structure of the decay. Furthermore, it has been proposed that decays to an excited state could be used as a consistency test for $0\nu\beta\beta$ in a ton-scale experiments using one isotope [2].

It should be noted that of all 11 nuclei observed to undergo $2\nu\beta\beta$ decay, only two of them, ^{100}Mo and ^{150}Nd, have been observed to undergo $2\nu\beta\beta$ decay to the first excited 0^+_1 state [3, 4]. This project began as an attempt to extend these measurements of transitions to excited states to include a third nucleus. ^{96}Zr was selected as the best candidate due to its high phase space and Q value: $Q_{\beta\beta}(0^+_0) = 3.35$ MeV for the ground state decay and $Q_{\beta\beta}(0^+_1) = 2.202$ MeV for the decay to the first excited 0^+ state. The ground state $2\nu\beta\beta$ decay for ^{96}Zr was measured by the NEMO-3 collaboration, producing an experimental result of $T_{1/2} = [2.35 \pm 0.14(\text{syst}) \pm 0.16(\text{stat})] \times 10^{19}$ yr [5].

II. EXPERIMENTAL METHOD

Decays to excited final states will decay to the ground nuclear state via γ-ray emission. For the case of the excited 0^+ and 2^+ decays discussed in this paper, the decays will progress through the $0^+ \to 2^+ \to 0^+_{g.s.}$ and $2^+ \to 2^+ \to 0^+_{g.s.}$ decay modes, respectively. These decay sequences form a unique experimental signature in the form of two coincident γ rays. In the case of ^{96}Zr's $2\nu\beta\beta$ decay to the first excited 0^+_1 state of ^{96}Mo, this produces a 778.2+369.8 keV coincidence. The present detection method relies on detecting both of these γ rays in coincidence to reduce experimental background and provide a high signal-to-background ratio.

A. Detector apparatus

The complete detector system is detailed in Ref. [4]. A brief overview of the system, as relevant to this paper, is given here. The heart of the detector system is two coaxial high-purity germanium (HPGe) detectors which sandwich a disk-shaped sample. Both p-type germanium crystals are 88 mm in diameter and 50 mm in length.

* sfinch@tunl.duke.edu

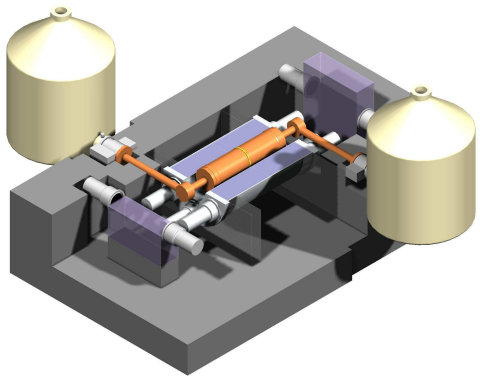

FIG. 1. (Color online) Diagram of the detector system. The copper plates are not shown and are located between the NaI annulus and lead shielding.

The HPGe detectors are surrounded by a NaI annulus 50 cm in length, interior diameter 12.5 cm, and exterior diameter 35.6 cm. Scintillation light is monitored by six 3" photomultiplier tubes (PMTs). In this experiment the NaI annulus is used as an active veto and Compton suppression shield. Additionally, two plastic scintillator end caps are positioned on each side of the annulus to provide additional veto power. Each plastic scintillator end cap is monitored by two 2" PMTs. A diagram of this apparatus is shown in Fig. 1.

The entire apparatus is surrounded by two layers of passive shielding: 0.75" oxygen-free high conductivity copper and 6" of lead. The passive shielding reduces much of the naturally occurring background radiation. The experimental apparatus is located in the Kimballton Underground Research Facility (KURF). The lab has an overburden of 520 m of dolomite and limestone, which provides 1450 m of water equivalent shielding from cosmic rays [6].

All signal processing is performed with NIM modules linked via coaxial cables. Five signals are recorded for each generation of the master trigger: the pulse height of each HPGe, the timing between the HPGes, and two copies of the veto timing.

Both detectors have their preamplifier output fed into a spectroscopic amplifier. The amplifier output is fed into an 11 bit EG&G Ortec analog-to-digital converter (ADC) computer automated measurement and control (CAMAC) module to record the pulse height and reconstruct the energy deposited in each detector. The timing pulses for both detectors are summed to form the master trigger for the ADC. The timing between the two detectors is measured with a time-to-amplitude converter (TAC), which inputs to the same CAMAC ADC. Every event originating in a HPGe detector is recorded and the coincidence criteria is enforced in software. The signals from the PMTs, both on the NaI annulus and the plastic end caps, are summed together to form a veto trigger. The veto trigger is measured by a TAC and records the timing between the master trigger and the veto trigger.

The CAMAC controller module and data acquisition are handled by a version of Jefferson Lab's continuous electron beam accelerator facility online data-acquisition (CODA) software modified for use at Triangle Universities Nuclear Laboratory (TUNL) [7]. The data are recorded on a Unix workstation and converted into ROOT TTrees using the program CODA2ROOT.

B. Enriched ^{96}Zr sample

As the natural abundance of ^{96}Zr is only 2.8%, samples enriched in ^{96}Zr were leased from Oak Ridge National Laboratory. Two powdered ZrO_2 samples of different enrichment were obtained. Since the efficiency of the two coaxial detector apparatus is the highest at the center of the detectors faces, the more enriched sample (#1) was concentrated at the center of the apparatus. This sample has a mass of 7.2835 g enriched to 91.4% ^{96}Zr, resulting in a mass of 4.987 g ^{96}Zr. The sample was packaged in an acrylic disk with 1.4 mm thick walls, a 31.75 mm diameter, and 10.22 mm high. The height of the sample mimics the dimensions of previous measurements [4]. Sample #2 has a mass of 26.9685 g oxide enriched to 64.2% ^{96}Zr, 12.927 g ^{96}Zr, and is housed in an annular acrylic container designed to encompass the more enriched sample. This container has a 69.95 mm outer diameter, 10.07 mm height, 1.31 mm radial walls, and 1.57 mm thick longitudinal walls. The two samples together total 17.914 g ^{96}Zr and were centered on the face of the coaxial detectors.

C. Data processing

Data are divided into runs, which are manually started and stopped approximately every 4 days. The ADC readout is calibrated to energy for each individual run using four background peaks: 238.6, 511.0, 1460.8, and 1764.5 keV. Even though each run is individually calibrated, we still observe excellent stability of $< \pm 0.5\%$ for the majority of runs without calibration. Each run is also examined for gain shifts that degrade detector resolution. Runs exhibiting such behavior are excluded from the analysis. Given the large time scale of the present experiment, the long term stability of the HPGe detectors was verified by monitoring the detector's count rate, energy resolution, and efficiency.

Data were collected over the course of 923 days from March 2012 to September 2014. Excluding detector downtime and runs which did not meet our data quality cuts, 685.7 days (1.877 yr) of data were produced, amounting to 74% detector live time.

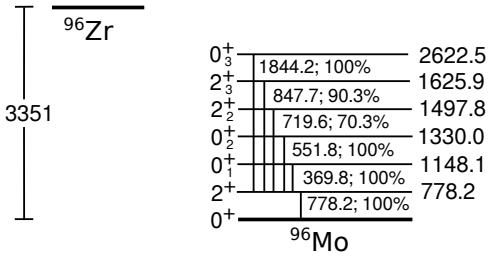

FIG. 2. The different excited states of ^{96}Mo following the $\beta\beta$ decay of ^{96}Zr. All energies given in keV. Figure not to scale.

III. DOUBLE-β DECAY OF ^{96}ZR

Due to its large Q value, there are many excited states in ^{96}Mo that ^{96}Zr could $2\nu\beta\beta$ decay through, as shown in Fig. 2. In each of these cases, the decays are assumed to proceed via the 2^+_0 state. The 2^+ states investigated have a small branching ratio directly to the ground state. As these decay modes would not benefit from the coincidence technique of the current experiment, only the $2^+ \rightarrow 2^+ \rightarrow 0^+$ decay mode is investigated, with the branching ratio indicated in the figure, in addition to the more likely $0^+ \rightarrow 2^+ \rightarrow 0^+$ decay.

A. Analysis

In the present analysis we require no events in the scintillator vetoes (a strict anti-coincidence) and a coincidence between the two HPGe detectors. Energy cuts were imposed on each HPGe detector corresponding to the ROI's γ-ray energy. Each HPGe is assumed to have a Gaussian energy resolution with standard deviation σ. Energy cuts were imposed as $\pm 2\sigma$ for both detectors. For the 369.8+778.2 keV $\gamma - \gamma$ coincidence resulting from $2\nu\beta\beta$ decay to the first excited 0^+_1 state, histograms are projected to show all events in coincidence with 369.8 keV and all events in coincidence with 778.2 keV. The result of these cuts is shown in Fig. 3

The background level in these histograms is extrapolated as a flat line around the region of interest (ROI). The background extrapolation region was taken as the largest peak-free region surrounding the ROI, ideally ± 100 keV. As the majority of background coincident events come from the Compton continuum, the flat background assumption accurately models the experimentally observed background.

This same procedure was followed to search for $2\nu\beta\beta$ decays to higher excited final states, as is shown in Fig. 4. In each case, the number of observed events in the ROI was consistent with the estimated background. There is a small background peak present to the left of the ROI for the 2622.5 keV state. This is created by Compton scattering of ^{208}Tl's 2614.5 keV γ ray. This background peak was incorporated into the background model for the 0^+_3 state.

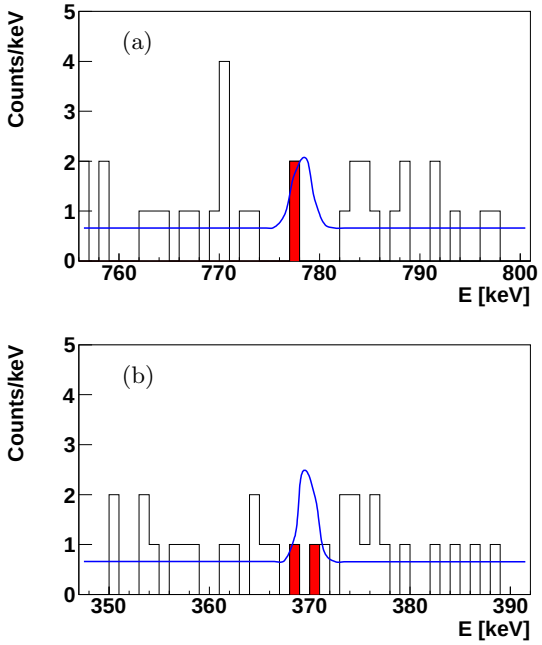

FIG. 3. (Color online) The $\beta\beta$ decay to the first excited 0^+ state region of interest with the ^{96}Zr sample in place (685.7 days). (a) shows events in coincidence with 369.8 keV and (b) shows events in coincidence with 778.2 keV. Events matching the $\gamma - \gamma$ coincidence criteria are highlighted in red. The minimum detectable signal above background at the 90% confidence level is shown by the blue curve.

The detector resolution was extracted from the production data set and was known to 0.8% uncertainty. This uncertainty, when propagated through the analysis code, produced a resulting 0.4% systematic uncertainty in the final experimental sensitivity. Given the low background rate of the experiment, the background model had a relatively high uncertainty, 11.9%. The background model resulted in a systematic uncertainty of 3.3% in the experimental sensitivity. These uncertainties combine to form a total systematic uncertainty of 3.4% for the analysis procedure to the 0^+_1 state. Similar results were produced for the decays to higher excited states.

B. Coincidence efficiency

The coincidence efficiency of the apparatus was measured using a ^{102}Rh source. This source was chosen because it exhibits the $0^+ \rightarrow 2^+ \rightarrow 0^+$ decay scheme of interest for $\beta\beta$ decay to excited states. Furthermore, it also exhibits a $2^+ \rightarrow 2^+ \rightarrow 0^+$ decay mode. ^{102}Rh has a half-life of 207.3 ± 1.7 days, making it convenient for efficiency measurements. The ^{102}Rh source was produced using the ^{102}Ru(p,n)^{102}Rh reaction with 5 MeV protons from the TUNL tandem accelerator. The activity of the source was determined by comparing its yield to that of a calibrated ^{137}Cs source.

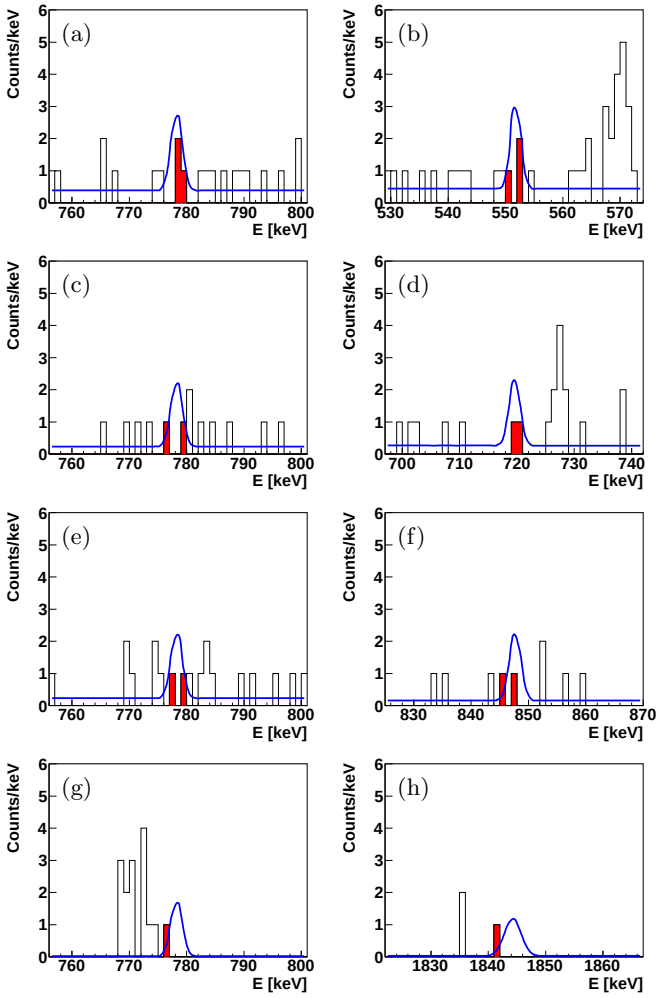

FIG. 4. (Color online) The region of interest for the $\beta\beta$ decay of ^{96}Zr to higher excited states. Events passing the cut criteria are highlighted red, with the expected signal at the given 90% confidence level shown by the blue curve. (a) and (b) show the 0_2^+ 778.2 + 551.8 keV coincidence, (c) and (d) show the 2_2^+ 778.2 + 719.6 keV coincidence, (e) and (f) show the 2_3^+ 778.2 + 847.8 keV coincidence, and (g) and (h) show the 0_3^+ 778.2 + 1844.3 keV coincidence.

The efficiency was measured as a function of radius for eight points between $0 \leq r \leq 4.5$ cm and is the average of four scans in different directions (up/down/left/right). The coincidence efficiency is shown in Fig. 5 with the size of the ^{96}Zr samples shown for comparison. The coincidence efficiency is fit to a function of the form

$$\epsilon(r) = \frac{a}{1 + br^2 + cr^4}\,. \tag{3}$$

The total efficiency involves the efficiency in the vicinity of both disks. This is evaluated as the product of the

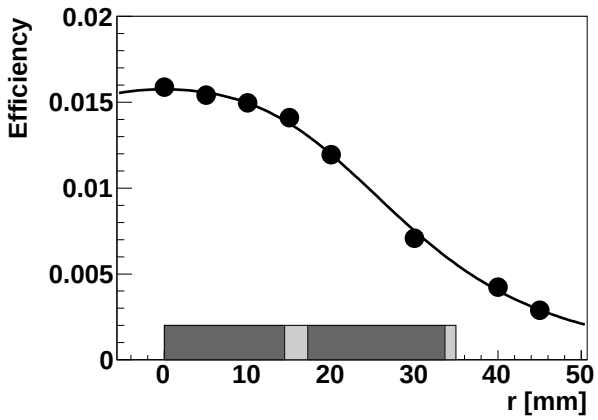

FIG. 5. Coincidence efficiency as a function of radius for the apparatus. The radial size of the two ZrO_2 samples and their holders is shown by the dark and light grey boxes, respectively.

efficiency and the mass of the ^{96}Zr samples:

$$N_0\epsilon = N_1 \frac{\int_0^{r_1} \epsilon(r) r dr}{\int_0^{r_1} r dr} + N_2 \frac{\int_{r_2}^{r_3} \epsilon(r) r dr}{\int_{r_2}^{r_3} r dr}\,. \tag{4}$$

Here, N_1 and N_2 are the number of ^{96}Zr nuclei in the inner and outer sample, respectively. r_1 is the radius of the inner disk, while r_2 and r_3 are the radii of the outer annular disk.

A number of corrections must be made to the ^{102}Rh measurement in order to be applicable to our measurement on ^{96}Zr. Firstly, HPGe detectors have a strong efficiency dependence on the energy of the incident γ ray. The efficiency as a function of energy was measured using a ^{152}Eu source and confirmed by GEANT4 simulations.

The difference in efficiency is calculated as the ratio between ^{96}Mo's 369+778 keV coincidence and ^{102}Ru's 468+475 keV coincidence:

$$\frac{\epsilon_{\gamma\gamma}(369,778)}{\epsilon_{\gamma\gamma}(468,475)} = \frac{\epsilon_{\gamma1}(369)\epsilon_{\gamma2}(778) + \epsilon_{\gamma1}(778)\epsilon_{\gamma2}(369)}{\epsilon_{\gamma1}(468)\epsilon_{\gamma2}(475) + \epsilon_{\gamma1}(475)\epsilon_{\gamma2}(468)}\,, \tag{5}$$

where the numerical subscripts refer to detector 1 and 2. When taking the ratio of two efficiencies, the systematic uncertainty of the ^{152}Eu source's activity cancels out, leaving a correction with a small relative uncertainty. The same procedure is performed for all coincidences of interest and is summarized in Table I.

The γ rays emitted by the sample will be attenuated by the sample itself. This effect may be accurately calculated by GEANT4 simulations. The efficiency measurements were taken when the apparatus was examining the $2\nu\beta\beta$ decay of ^{100}Mo. In order to accurately reproduce the attenuation of the ^{100}Mo sample, 5 mm of ^{nat}Mo metal were placed on both sides of the ^{102}Rh point

TABLE I. Efficiency-correction ratios for different coincidences in ^{96}Mo. The attenuation ratio of the ^{96}Zr sample and the energy dependence ratio of the detectors are both given.

J^π	γ_1 [keV]	γ_2 [keV]	Sample attenuation	$\epsilon(\gamma_1,\gamma_2)/\epsilon(468,475)$
0_1^+	369.7	778.2	0.851 ± 0.001	0.827 ± 0.003
0_2^+	551.8	778.2	0.868 ± 0.001	0.615 ± 0.006
2_2^+	719.6	778.2	0.875 ± 0.001	0.506 ± 0.007
2_3^+	847.7	778.2	0.881 ± 0.002	0.448 ± 0.007
0_3^+	1844.3	778.2	0.897 ± 0.002	0.252 ± 0.007

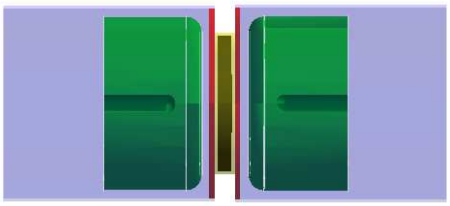

FIG. 6. (Color online) The two-coaxial HPGe apparatus as modeled in GEANT4. The ^{96}Zr sample is shown in between the detectors.

source. A GEANT4 simulation was run with the detector geometry, point source, and metal disk accurately reproduced. The ratio of full energy coincidence counts in the ^{102}Rh region of interest with and without the metal disk gives an attenuation ratio. Although the attenuation ratio varies as a function of position, it is ≈3.27. Each data point in Fig. 5 has been corrected by this method to accurately reflect the efficiency with no sample attenuation. The same procedure was also performed in order to calculate the attenuation in the ^{96}Zr sample. The GEANT4 reconstruction of the ^{96}Zr samples in between the two coaxial detectors is shown in Fig. 6. The attenuation results are summarized in Table I.

The separation distance between the two detectors can have a noticeable effect on the efficiency, as it is strongly correlated with the solid angle covered by the detectors. The efficiency measurements were done with an 11 mm separation distance. In the ^{96}Zr experiment, the detectors are separated by the thickness of the sample: 10.22 mm. This effect was simulated using GEANT4. This results in a change of efficiency of

$$\frac{\epsilon(d=10.22)}{\epsilon(d=11.0)} = 1.022 \pm 0.0014\,. \qquad (6)$$

Finally, a GEANT4 simulation was conducted to determine the effect of the sample's spatial extent along the Z-axis. The efficiency data are taken with a point source located at $Z = 0$ mm. Our sample has a thickness of approximately 7 mm, so the actual decays will be uniformly distributed from $-3.5 < Z < 3.5$ mm. The GEANT4 simulation was performed for both of these conditions. This resulted in a ratio of efficiencies of

$$\frac{\epsilon(-3.5<Z<3.5)}{\epsilon(Z=0)} = 0.9998 \pm 0.0014\,. \qquad (7)$$

As no effect was seen at the level of statistical significance, this ratio was assumed to be unity, although the uncertainty is added into the final error budget.

For $\beta\beta$ decay to excited states, only the 0^+ and 2^+ states may be populated. As such, only the $0^+ \to 2^+ \to 0^+$ and $2^+ \to 2^+ \to 0^+$ decay sequences are of interest. The effects of the different decay modes may be accurately studied using GEANT4, as all the decay parameters are set by theory. The results of this simulation were in good agreement with the measured EC decay of ^{102}Rh to the 2_2^+ state after corrections for the energy dependence are made.

The error budget for the efficiency is shown in Table II. The largest source of error (3.1%) comes from the calibrated ^{137}Cs source that was used to determine the total detector efficiency. The second largest effect (2.5%) comes from the uncertainty in the detector and source placement. The only other sizable contribution to the error budget (2.4%) stems from small asymmetries discovered when measuring the radial efficiency. This is incorporated here through evaluations of the uncertainty in the fit of Fig. 5. The systematic error on the apparatus efficiency (5.0%) may be added with the systematic uncertainty resulting from the analysis procedure (3.4%), which results in a total uncertainty of 6.0%.

TABLE II. The systematic error budget for the apparatus's efficiency. These uncertainties are for the decay to the first excited 0_1^+ state. Note that uncertainty on the energy dependence and attenuation correction factors is energy dependent and will be higher for the decays to higher excited states.

Uncertainty contribution	Percent error
Calibration of ^{137}Cs source	3.1 %
Energy dependence correction factor	0.4 %
Attenuation correction factor	0.2 %
Z dependence correction factor	0.15 %
Detector and source geometry	3.0 %
Non-symmetrical efficiency curve	2.4 %
Dead time	0.15 %
Uncertainty in ^{102}Rh half-life	0.82 %
Total uncertainty	5.0 %

C. Limit setting

Lower limits were set using the formula

$$T_{1/2} > \ln 2 \frac{t f_b N_0 \epsilon_{\gamma\gamma}^{tot}}{N_d}\,, \qquad (8)$$

where t is the exposure time, f_b is the branching ratio, N_0 is the number of nuclei, $\epsilon_{\gamma\gamma}^{tot}$ is the efficiency with all the corrections discussed in the previous chapters,

and N_d is a statistical factor representing the number of counts above background to which the experiment is sensitive. N_d was calculated using the method of Feldman and Cousins [8] for a Poisson process and a 90% confidence level. The systematic uncertainty on the efficiency is included in limit setting at the 90% confidence level. In the case that the number of observed counts is less than the expected background, the Feldman-Cousins sensitivity is given in addition to the confidence limit. The sensitivity is only a function of the expected background and is the mean limit that would be measured by a collection of experiments with no true signal. The resulting limits are shown in Table III.

Previous searches for this decay were performed with a single HPGe detector [9, 11] searching for single de-excitation γ rays. As such, this is the first experimental result for the $2\nu\beta\beta$ decay of ^{96}Zr to excited states using a coincidence technique. The previous best limits used a well-type HPGe to monitor 8.0 g of ^{96}Zr for 464.4 hours [9]. The high solid-angle average and efficiency of the detector produced very competitive limits. This technique has several drawbacks, including much larger background levels, necessary corrections for coincident summing in the well-type detector, and a very short run time. Furthermore, and contrary to our approach, the result of Refs. [9, 11] could potentially be contaminated by two successive single-β decays of ^{96}Zr, which also produces the final excited 2^+ state of ^{96}Mo. Its experimentally unknown half-life time may be of the same order as that for the $2\nu\beta\beta$ decay of ^{96}Zr [12]. These concerns are addressed with the coincidence experiment conducted in the present work and result in limits a factor of 5 better for the decay to the 0_1^+ state and a factor of 2 better for the two 2^+ states.

Concluding this section, we note that a natural zirconium sample was also investigated. Metal sheets of ^{nat}Zr, totaling 10 mm thick, 10.0 cm in diameter, and 430 g were counted for 0.438 yr (160 days) using the same detector apparatus. This amounts to 12.03 g of ^{96}Zr. The ^{nat}Zr sample was found to contain large impurities of ^{235}U and its daughters. Although this background would overwhelm most experiments aimed at detecting single γ rays, the coincidence ROI was not effected and eliminated need for a clean sample. The effective efficiency for ^{nat}Zr ROI is 2.92 times smaller than the enriched sample efficiency, mostly due to the higher γ ray attenuation by the denser metal sample. Data acquired with the natural zirconium sample produced a 90% sensitivity of $T_{1/2} > 2.4\times10^{19}$ for the decay to the 0_1^+ state, 11 times smaller than the sensitivity limit produced with the enriched sample, thus illustrating the benefits of using the isotopically enriched sample.

IV. CONCLUSIONS

A systematic law for the $\beta\beta$-decay half-lives, published by Ren and Ren [10], is used to produce estimates for the excited state decays. This law is fit to experimental data for the ground state decay, but was shown to produce accurate results for decays to the first excited 0^+ state. The law agreed within the experimental error for the decay of ^{100}Mo to the 0_1^+ state. The law underestimated the half-life of ^{150}Nd by 30-70%, although the experimental errors are large and the nuclear deformation of ^{150}Nd is not taken into account. Our experimental limit exceeds the prediction of Ref. [10] by 25% and excludes this prediction at the 93% confidence level. The quasiparticle random phase approximation (QRPA) was used to calculate theoretical half-lives of 3.8×10^{21} yr [13] and $2.4-2.7\times10^{21}$ yr [14] for the decay to the 0_1^+ state. Furthermore, the 2_2^+ state was theoretically calculated to have a half-life of $6.0-6.3\times10^{24}$ yr [14]. Although the systematic law produces promising results, these theoretical calculations indicate that an additional order of magnitude sensitivity is needed for observation of the decay.

A limit on the decay's NME may be extracted using Eq. (2) and the phase-space factor given in Ref. [15]. This results in a limit on the NME $|M^{2\nu}_{eff}(0_1^+)| < 0.13$ at the 90% confidence level. Unfortunately, this is not strict enough to test the calculation of Ref. [16], who calculated $|M^{2\nu}(0_1^+)| = 0.04$. Their reported calculation was done using the closure approximation, which is often disfavored for the single-state dominance (SSD) hypothesis for the $2\nu\beta\beta$ decay mode. It would be interesting to see how this limit compared to a calculation performed using the SSD hypothesis.

The present experimental apparatus has now investigated the $2\nu\beta\beta$ decay to the first excited 0_1^+ state for three different nuclides. The results of these three studies are summarized in Table IV. These three nuclides have the largest phase-space factors for the decay to the first excited 0^+ state and, as such, are the best candidate for $2\nu\beta\beta$ decay to excited state studies.

Strict limits for the $2\nu\beta\beta$ decay of ^{130}Te to the first 0^+ excited state were set by the CUORICINO collaboration [18]. Their experiment also relied on a γ coincidence method and produced limits of 1.3×10^{23} yr. Although their limit is ≈ 420 times greater than the present result, the first excited 0^+ state of ^{130}Xe occurs at 1793.5 keV. The small Q value results in ^{130}Te having a phase-space factor ≈ 230 times smaller than ^{96}Zr. The resulting limits on the respective NMEs are comparable for the two experiments. The present limits for ^{96}Zr were limited by the small sample size of 17.9 g. For comparison, the limits of CUORICINO were produced with a 11.3 kg target mass.

ACKNOWLEDGMENTS

This work was supported in part by the US Department of Energy, Office of Nuclear Physics under Grant No. DE-FG02-ER41033. The authors would like to thank R.B. Vogelaar and S.D. Rountree for their role in

TABLE III. The 90% half-life confidence limits (C.L.) and experimental sensitivity for the $2\nu\beta\beta$ decay of ^{96}Zr to excited states in ^{96}Mo extracted from the present experimental data. Previous best limits and a systematic estimate for the lifetime are also given.

J^π	E [keV]	f_b	$T_{1/2}$ [yr] This work 90% C.L.	This work 90% Sensitivity	Previous work 90% C.L.[9]	Systematic law [10]
0_1^+	1148.1	1.00	$> 3.1 \times 10^{20}$	$> 2.7 \times 10^{20}$	$> 6.8 \times 10^{19}$	2.59×10^{20}
0_2^+	1330.0	1.00	$> 1.4 \times 10^{20}$	-	-	4.29×10^{20}
2_2^+	1497.8	0.703	$> 1.0 \times 10^{20}$	-	$> 6.1 \times 10^{19}$	7.42×10^{20}[a]
2_3^+	1625.9	0.903	$> 1.2 \times 10^{20}$	-	$> 5.4 \times 10^{19}$	1.21×10^{21}[a]
0_3^+	2622.5	1.00	$> 1.1 \times 10^{20}$	$> 1.0 \times 10^{20}$	-	2.08×10^{25}

[a] The method of Ref. [10] is not calibrated to decays to 2^+ states and may not produce reliable estimates for these decay modes.

TABLE IV. Experimentally extracted nuclear matrix elements for $2\nu\beta\beta$ decay to the excited 0_1^+ state. The three searches performed by the present apparatus are summarized.

Nuclide	$T_{1/2}$ [yr]	$\lvert M_{eff}^{2\nu}(0_1^+)\rvert$
^{96}Zr	$> 3.1 \times 10^{20}$	> 0.13
^{100}Mo	$[5.5^{+1.2}_{-0.8}(\text{stat})\pm 0.3(\text{syst})] \times 10^{20}$	$0.172^{+0.019}_{-0.013}$ [17]
^{150}Nd	$[1.07^{+0.45}_{-0.25}(\text{stat})\pm 0.07(\text{syst})] \times 10^{20}$	$0.0465^{+0.0098}_{-0.0054}$ [4]

establishing and maintaining KURF. The authors would also like to thank Bret Carlin for his networking experience.

[1] F. T. Avignone, S. R. Elliott, and J. Engel, Rev. Mod. Phys. **80**, 481 (2008).
[2] M. Duerr, M. Lindner, and K. Zuber, Phys. Rev. D **84**, 093004 (2011).
[3] A. S. Barabash, Phys. Rev. C **81**, 035501 (2010).
[4] M. F. Kidd, J. H. Esterline, S. W. Finch, and W. Tornow, Phys. Rev. C **90**, 055501 (2014).
[5] J. Argyrlades *et al.* (NEMO-3 Collaboration), Nucl. Phys. A **847**, 168 (2010).
[6] P. Finnerty *et al.*, Nucl. Instrum. Methods A **642**, 65 (2011).
[7] M. W. Ahmed, C. R. Howell, and A. S. Crowell, *CODA at TUNL (C@T) and the TUNL Real-Time Analysis Package (TRAP) Version 03.a* (2014), http://www.tunl.duke.edu/ daq/tunldaq.html.
[8] G. J. Feldman and R. D. Cousins, Phys. Rev. D **57**, 3873 (1998).
[9] A. S. Barabash, R. Gurriarán, F. Hubert, J. L. Reyss, J. Suhonen, and V. I. Umatov, J. Phys. G **22**, 487 (1996).
[10] Y. Ren and Z. Ren, Phys. Rev. C **89**, 064603 (2014).
[11] C. Arpesella, A. S. Barabash, E. Bellotti, C. Brofferio, E. Fiorini, P. P. Sverzellati, and V. I. Umatov, Europhys. Lett. **27**, 29 (1994).
[12] H. Heiskanen, M. T. Mustonen, and J. Suhonen, J. Phys. G **34**, 837 (2007).
[13] S. Stoica and I. Mihut, Nucl. Phys. A **602**, 197 (1996).
[14] J. Toivanen and J. Suhonen, Phys. Rev. C **55**, 2314 (1997).
[15] J. Kotila and F. Iachello, Phys. Rev. C **85**, 034316 (2012).
[16] J. Barea, J. Kotila, and F. Iachello, Phys. Rev. C **87**, 014315 (2013).
[17] M. F. Kidd, J. H. Esterline, W. Tornow, A. S. Barabash, and V. I. Umatov, Nucl. Phys. A **821**, 251 (2009).
[18] E. Andreotti *et al.*, Phys. Rev. C. **85**, 045503 (2012).